neonSoilFlux: An R Package for Continuous Sensor-Based Estimation of Soil CO_2 Fluxes

John Zobitz[1] Ed Ayres[2] Zoey Werbin[3] Ridwan Abdi[1]
Natalie Ashburner-Wright[4] Lillian Brown[4]
Ryan Frink-Sobierajski[4] Lajntxiag Lee[1] Dijonë Mehmeti[1]
Christina Tran[4] Ly Xiong[1] Naupaka Zimmerman[4,5]

[1] Augsburg University, 2211 Riverside Avenue, Minneapolis, MN 55454

[2] National Ecological Observatory Network, Battelle, 1685 38th Street, Suite 100, Boulder, CO 80301

[3] Boston University, 5 Cummington Street, Boston, MA 02215

[4] University of San Francisco, 2130 Fulton Street, San Francisco, CA 94117

[5] University of Kansas, 1251 Wescoe Dr. Lawrence, KS 66045

Acknowledgments

JZ acknowledges Kathleen O'Rourke for code development. NZ thanks technical staff at USF for support with field gear assembly and shipping. We thank the NEON field staff and assignable assets teams for facilitating each of the six NEON site visits. We are grateful to LI-COR technical staff for helpful discussions about optimal sampling methods. This work was supported by NSF DEB grant #2017829 awarded to JZ, and NSF DEB grant #2017860 awarded to NZ. This material is based in part upon work supported by the National Ecological Observatory Network (NEON), a program sponsored by the U.S. National Science Foundation (NSF) and operated under cooperative agreement by Battelle.

Conflict of Interest Statements

None of the authors have a financial, personal, or professional conflict of interest related to this work.

Author Contributions

Conceptualization: JZ, NZ; Methodology: EA, JZ, NZ; Software: JZ, NZ, ZW, E A, DM, RA, LX, LL; Validation: JZ, NZ; Formal Analysis: JZ, NZ, DM, RA, LX, LL; Investigation: JZ, NZ, RF-S, CT, NA-W, LB; Resources: JZ, NZ; Data curation: JZ, NZ, DM, LX; Writing – original draft: JZ, NZ; Writing – review and editing: JZ, NZ, ZW, EA, CT, DM, LX,; Visualization: JZ, NZ, DM, RA, LX; Supervision: JZ; NZ; Project Administration: JZ; NZ; Funding Acquisition: JZ; NZ

Data Availability

Data available will be made available via Zenodo prior to publication.

1 Abstract

Accurate quantification of soil carbon fluxes is essential to reduce uncertainty in the terrestrial carbon sink. These fluxes vary over time and across ecosystem types. The flux gradient method estimates soil carbon fluxes using paired measurements of soil CO_2 concentration, temperature, moisture, and other soil properties. The National Ecological Observatory Network (NEON) provides such data across 20 ecoclimatic domains spanning the continental U.S., Puerto Rico, Alaska, and Hawai‘i. We present an R software package (`neonSoilFlux`) that acquires soil environmental data to compute half-hourly soil carbon fluxes for each soil replicate plot at a terrestrial NEON site. To assess the computed fluxes, we visited six focal NEON sites and measured soil carbon fluxes using a closed-dynamic chamber approach. Outputs from the `neonSoilFlux` showed order-of-magnitude agreement to measured fluxes (R^2 between measured and `neonSoilFlux` outputs ranging from 0.00 to 0.78), but fell within the range of calculated uncertainties. Calculated fluxes from `neonSoilFlux` aggregated to the daily scale exhibited expected site-specific seasonal patterns. While the flux gradient method is broadly effective, its accuracy is highly sensitive to site-specific inputs, particularly estimates of soil diffusivity and moisture content. Future refinement and validation of `neonSoilFlux` outputs can contribute to existing databases of soil carbon flux measurements, providing near real-time estimates of a critical component of the terrestrial carbon cycle.

1.1 Keywords

Soil carbon, carbon dioxide, flux gradient, carbon cycle, field validation, soil respiration, ecosystem variability, diffusion

2 Data for peer review

Anonymous data and code for peer review is available here: LINK

3 Introduction

Soils contain the largest reservoir of terrestrial carbon (Jobbágy & Jackson, 2000). A critical component of this reservoir is soil organic matter, the accumulation of which is influenced by biotic factors such as above-ground plant inputs (Jackson et al., 2017). These inputs in turn are influenced by environmental factors such as growing season length, temperature, and moisture (Desai et al., 2022), which also affect the breakdown of soil organic matter and its return to the atmosphere. Across heterogeneous terrestrial landscapes, the interplay between these biotic and abiotic factors influence the size of the soil contribution to the terrestrial carbon sink (Friedlingstein et al., 2025). However, the heterogeneity of these processes across diverse ecosystems in the context of rapid environmental change leads to large uncertainty in the magnitude of this sink in the future, and thus a pressing need to quantify changes in soil carbon pools and fluxes across scales.

Ecological observation networks such as the United States' National Ecological Observatory Network (NEON) and others (e.g. FLUXNET or the Integrated Carbon Observation System) present a significant advancement in the nearly continuous observation of biogeochemical processes at the continental scale. Notably, at 47 terrestrial sites across the continental United States, NEON provides half-hourly measurements of soil CO_2 concentration, temperature, and moisture at different vertical depths. Each of these NEON sites also encompasses measurements of the cumulative sum of all ecosystem carbon fluxes in an airshed using the eddy covariance technique (Baldocchi, 2014). Soil observations provided by NEON are on the same timescale and standardized with eddy covariance measurements from FLUXNET. These types of nearly continuous observational data (NEON and FLUXNET) can be used to reconcile differences between model-derived or data-estimated components of ecosystem carbon flux (Jian et al., 2022; Luo et al., 2011; Phillips et al., 2017; J. Shao et al., 2015; P. Shao et al., 2013; Sihi et al., 2016).

Estimated or observed soil carbon fluxes are a key metric for understanding change in soil carbon pools over time (Bond-Lamberty et al., 2024). A soil carbon flux to the atmosphere (F_S, units μmol m^{-2} s^{-1}), represents the aggregate process of transfer of soil CO_2 to the atmosphere from physical and biological processes (e.g. diffusion and respiration). Soil carbon fluxes can be assumed to encompass soil carbon respiration from autotrophic or heterotrophic sources (Davidson et al., 2006) and modeled with a exponential Q_{10} paradigm (Bond-Lamberty et al., 2004; Chen & Tian, 2005; Hamdi et al., 2013).

One common method by which F_S is measured in the field is through the use of soil chambers in a closed, well-mixed system (Norman et al., 1997) with headspace trace gas concentrations measured with an infrared gas analyzer (IRGA). F_S can also be estimated from soil CO_2 measurements at different depths in the soil using the flux-gradient method (Maier & Schack-Kirchner, 2014). Closed-chamber IRGA measurements require either frequent in-person site visits or an expensive automated systems; the flux-gradient method is calculated from using solid-state sensors. The flux-gradient method is an approach that uses conservation of mass to calculate flux at a vertical soil depth z at steady state by applying Fick's law of diffusion. A simplifying assumption for the flux-gradient method is that there is no mass transfer in the other spatial dimensions x and y (Maier & Schack-Kirchner, 2014). The diffusivity profile, a key component of this calculation, varies across the soil depth as a function of soil temperature, soil volumetric water content, atmospheric air pressure, and soil bulk density (Millington & Shearer, 1971; Moldrup et al., 1999; Sallam et al., 1984).

Databases such as the Soil Respiration Database (SRDB) or the Continuous Soil Respiration Database (COSORE) add to the growing network of resources for making collected observations of soil fluxes available to other researchers (Bond-Lamberty, 2018; Bond-Lamberty et al., 2020; Bond-Lamberty & Thomson, 2010; Jian et al., 2021; Jiang et al., 2024). However, these databases currently encompass primarily direct soil measurements of fluxes (i.e. those using methods like the closed-chamber method described above). Currently, NEON provides all measurements to calculate F_S from Fick's law, but soil flux as a derived data product was descoped from the initial network launch due to budget constraints (Berenbaum et al., 2015). Deriving estimates of F_S using continuous sensor data across NEON sites thus represents a high priority.

This study describes the application of an R software package, `neonSoilFlux`, that computes a standardized estimate of F_S at all terrestrial NEON sites using the flux-gradient method. Using direct chamber-based field observations of soil carbon dioxide flux from a subset of terrestrial NEON sites spanning six states, we provide a direct validation of F_S from `neonSoilFlux`.

Key objectives of this study are to:

1. Apply the flux-gradient method to estimate soil CO_2 flux from continuous sensor measurements across six NEON sites.
2. Benchmark estimated soil carbon fluxes against field measurements (e.g. direct chamber measurements of soil flux).
3. Identify sources of error in the flux-gradient approach across diverse sites in order to guide future work.

4 Materials and Methods

4.1 Field methods

4.1.1 Focal NEON Sites

In order to acquire field data to validate model predictions of flux, we selected six terrestrial NEON sites for analysis. We conducted field measurement campaigns at these sites, which span a range of environmental gradients and terrestrial domains (Table 1). SJER, SRER, and WREF were visited during May and June of 2022, and WOOD, KONZ, and UNDE during May and June of 2024.

Over the course of two field campaigns in 2022 and 2024, we conducted week-long visits at each site. In consultation with NEON field staff, we first selected a specific plot in the soil sampling array to maximize the concurrent availability of sensor data.

4.1.2 Soil collar placement

Either one (2022 sampling campaign) or two (2024 sampling campaign) PVC soil collars (20.1 cm inside diameter) were installed in close proximity to the permanent NEON soil sensors at each site (Figure 1). The soil plot where measurements were taken was chosen at each site in consultation with NEON staff to maximize likelihood of quality soil sensor measurements during the duration of the IRGA measurements at each site. After installation, collar(s) were left to equilibrate for approximately 24 hours prior to measurements being taken.

4.1.3 Infrared gas analyzer measurements of soil CO_2 flux

In 2022, we then made measurements of flux on an hourly interval for 8 hours each day. Measurements were taken from roughly 8 am to 4 pm, with the time interval selected to capture the majority of the diurnal gradient of soil temperature each day. These measurements were made using a LI-6800 infrared gas analyzer instrument (LI-COR Environmental, Lincoln, NE) fitted with a soil chamber attachment (attachment 6800-09). In 2024, we again used the same LI-6800 instrument, but made half-hourly measurements over an approximately 8 hour period. In addition, we also installed a second collar and used a second instrument, an LI-870 CO_2 IRGA, connected to an automated robotic chamber (LI-COR chamber 8200-104) controlled by an LI-8250 multiplexer, to make automated measurements. The multiplexer was configured to take half-hourly measurements 24 hours a day for the duration of our sampling bout at each site. Each instrument was paired with a soil temperature and moisture probe (Stevens HydraProbe, Stevens Water, Portland, OR) that was used to make soil temperature and moisture measurements concurrent with the CO_2 flux measurements. Chamber volumes were set by measuring collar offsets at each site. System checks were conducted daily for the LI-6800 and weekly for the LI-8250. Instruments were factory calibrated before each field season.

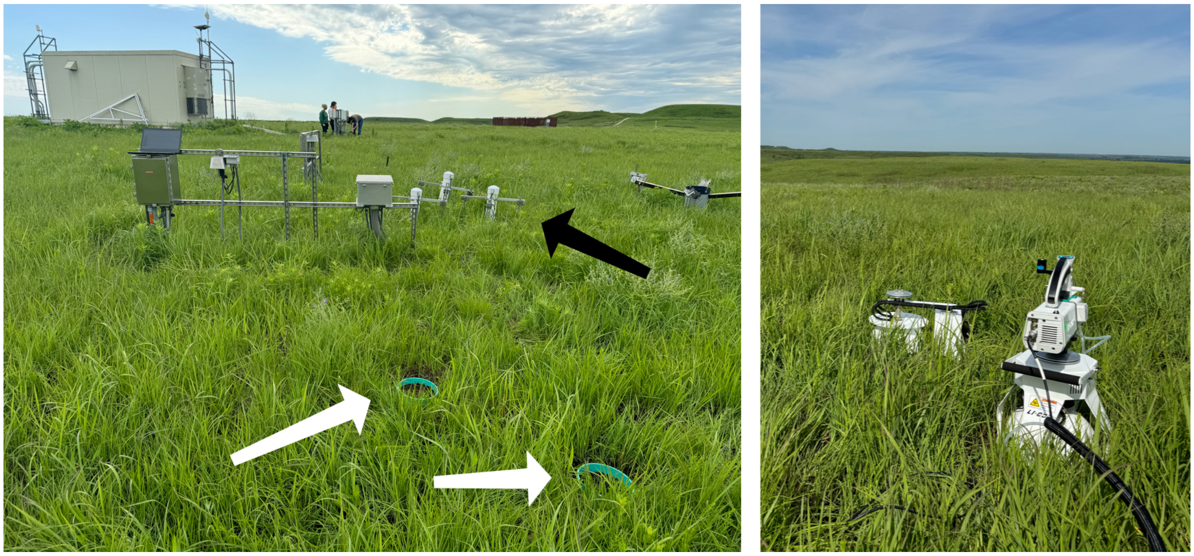

Figure 1: Spatial layout of field sampling using a closed-dynamic chamber setup at a representative NEON site (KONZ). Left image shows collars (white arrows) and permanent soil sensor installation (black arrow) and right image shows the LI-6800 (foreground) and LI-8200-104 (background) instruments placed on the collars.

Table 1: Listing of NEON sites studied for field work and analysis. $\overline{T_S}$: average soil temperature during field measurements. $\overline{SWC}$: average soil water content during field measurements. Soil plot refers to the particular location in the soil sensor array (denoted as HOR by NEON) where field measurements were made.

Site (NEON site ID)	Location	Ecosystem type	Mean annual temperature	$\overline{T_S}$ (°)	Mean annual precipitation	$\overline{SWC}$ (%)	Field measurement dates	Soil plot
Santa Rita Experimental Range (SRER)	31.91068, -110.83549	Shrubland	19.3°C	47.6°	346 mm	4.0%	29 May 2024 - 01 June 2024	004

Table 1: Listing of NEON sites studied for field work and analysis. $\overline{T_S}$: average soil temperature during field measurements. $\overline{SWC}$: average soil water content during field measurements. Soil plot refers to the particular location in the soil sensor array (denoted as HOR by NEON) where field measurements were made.

Site (NEON site ID)	Location	Ecosystem type	Mean annual temperature	$\overline{T_S}$ (°)	Mean annual precipitation	$\overline{SWC}$ (%)	Field measurement dates	Soil plot
San Joaquin Experimental Range (SJER)	37.10878, -119.73228	Oak woodland	16.4°C	41.7°	540 mm	1.2%	01 June 2022 - 04 June 2022	005
Wind River Experimental Forest (WREF)	45.82049, -121.95191	Evergreen forest	9.2°C	15.3°	2225 mm	27.2%	07 June 2022 - 09 June 2022	001
Chase Lake National Wildlife Refuge (WOOD)	47.1282, -99.241334	Restored prairie grassland	4.9°C	14.9°	495 mm	14.9%	03 June 2024 - 09 June 2024	001
Konza Prairie Biological Station (KONZ)	39.100774, -96.563075	Tallgrass Prairie	12.4°C	23.4°	870 mm	23.4%	29 May 2024 - 01 June 2024	001

Table 1: Listing of NEON sites studied for field work and analysis. $\overline{T_S}$: average soil temperature during field measurements. $\overline{SWC}$: average soil water content during field measurements. Soil plot refers to the particular location in the soil sensor array (denoted as HOR by NEON) where field measurements were made.

Site (NEON site ID)	Location	Ecosystem type	Mean annual temperature	$\overline{T_S}$ (°)	Mean annual precipitation	$\overline{SWC}$ (%)	Field measurement dates	Soil plot
University of Notre Dame Environmental Research Center (UNDE)	46.23391, -89.537254	Deciduous forest	4.3°	13.0°	802 mm	13.0%	22 May 2024 - 25 May 2024	004

4.1.4 Post-collection processing of field data

We used LI-COR SoilFluxPro software (v 5.3.1) to assess the data after collection and to inform sampling parameters. We checked appropriateness of dead band and measurement durations using built-in evaluation tools. Based on this, the deadband period was set for 30-40 seconds, depending on the site, and the measurement duration was 180 seconds with a 30 second pre-purge and a 30 second post-purge at most sites, and a 90 sec pre- and post-purge at sites with higher humidity due to recent precipitation events. We also assessed the R^2 of linear and exponential model fits to measured CO_2 to verify measurement quality.

4.2 neonSoilFlux R package

We developed an R package (neonSoilFlux; Zobitz et al. (2024)) to compute half-hourly soil carbon fluxes and uncertainties from NEON data. The objective of the neonSoilFlux package is a unified workflow (Figure 2) for soil data acquisition and analysis that supplements the existing data acquisition R package (https://CRAN.R-project.org/package=neonUtilities; Lunch et al. (2025)).

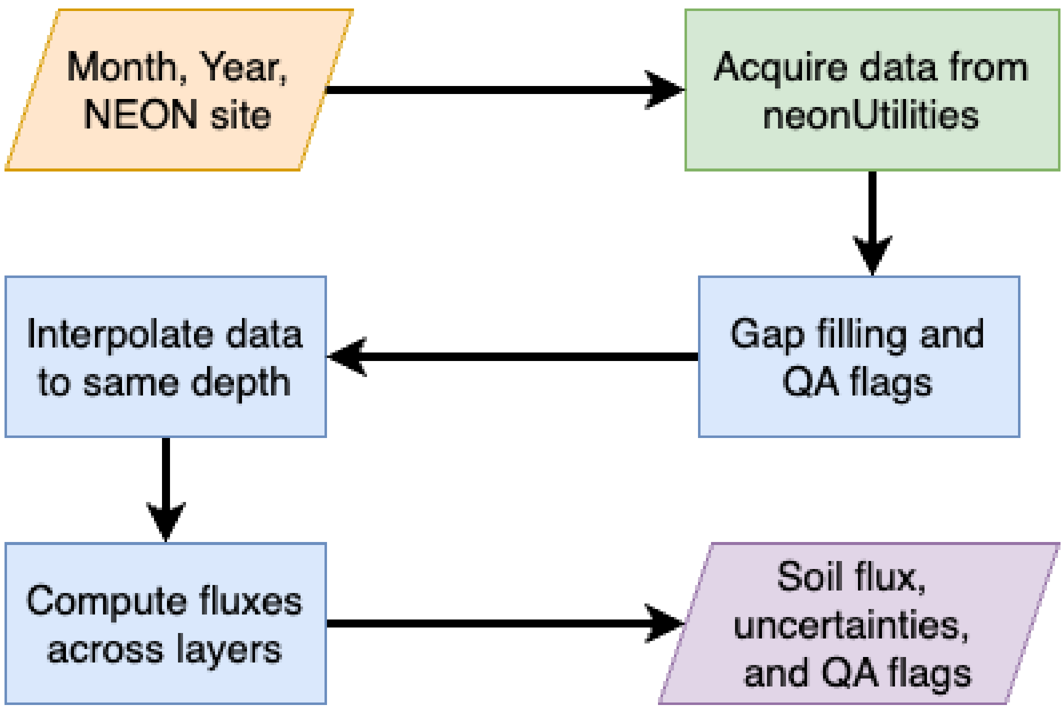

Figure 2: Diagram of neonSoilFlux R package. For a given month, year, and NEON site (orange parallelogram), the package acquires all relevant data to compute F_S using the neonUtilities R package (green rectangle). Data are gap-filled according to reported QA flags and interpolated to the same measurement depth before computing the soil flux, uncertainties, and final QA flags (blue rectangles). The package reports the associated soil flux, uncertainties, and quality assurance (QA) flags for the user (purple parallelogram).

At a given NEON site there are five replicate soil plots, each with measurements of soil CO_2 concentration, soil temperature, and soil moisture at different depths (Figure 3). The `neonSoilFlux` package acquires measured soil water content (National Ecological Observatory Network (NEON), 2024e), soil CO_2 concentration (National Ecological Observatory Network (NEON), 2024b), barometric pressure from the nearby tower (National Ecological Observatory Network (NEON), 2024a), soil temperature (National Ecological Observatory Network (NEON), 2024d), and soil properties (e.g. bulk density) (National Ecological Observatory Network (NEON), 2024c). The static soil properties were collected from a nearby soil pit during site characterization and are assumed to be constant at each site. A soil flux calculation is computed at each replicate soil plot.

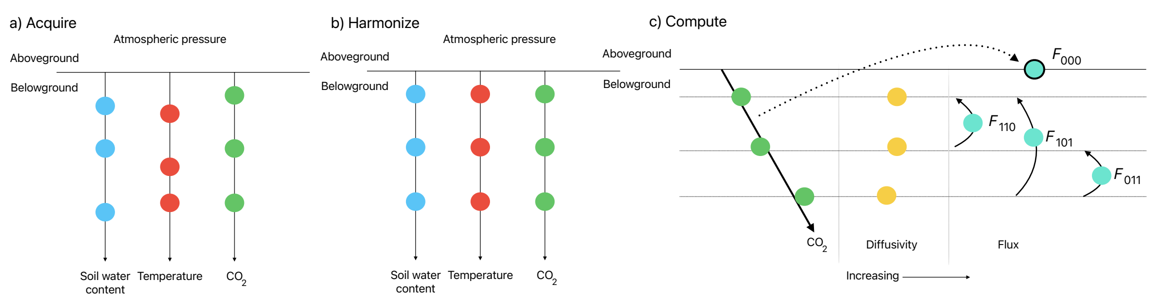

Figure 3: Model diagram for data workflow for the `neonSoilFlux` R package. a) Acquire: Data are obtained from given NEON location and horizontal sensor location, which includes soil water content, soil temperature, CO_2 concentration, and atmospheric pressure. All data are screened for quality assurance; if gap-filling of missing data occurs, it is flagged for the user. b) Any belowground data are then harmonized to the same depth as CO_2 concentrations using linear regression. c) The flux across a given depth is computed via Fick's law, denoted with F_{ijk}, where i, j, or k are either 0 or 1 denoting the layers the flux is computed across (i = closest to surface, k = deepest). F_{000} represents a flux estimate where the gradient dC/dz is the slope of a linear regression of CO_2 with depth.

The workflow to compute a value of F_S with `neonSoilFlux` consists of three primary steps, illustrated in Figure 3. First, NEON data are acquired for a given site and month via the `neonUtilities` R package (yellow parallelogram and green rectangle in Figure 2 and Panel a in Figure 3). Acquired environmental data can be exported to a comma separated value file for additional analysis. Quality assurance (QA) flags are reported as an indicator variable.

The second step is harmonizing the data to compute soil fluxes across soil layers. This step consists of three different actions (blue rectangles in Figure 2 and Panel b in Figure 3). If a given observation by NEON is reported as not passing a quality assurance check, we applied a gap filling method to replace that measurement with its monthly mean at that same depth (Section 4.2.1). Belowground measurements of soil water and soil temperature are then interpolated to the same depth as soil CO_2 measurements. The diffusivity (Section 4.2.2) and soil flux across different soil layers (Section 4.2.3) are then computed.

The third and final step is computing a surface soil flux through extrapolation to the surface (purple parallelogram in Figure 2 and Panel c in Figure 3). Uncertainty on a soil flux measurement is computed through quadrature. An aggregate quality assurance (QA) flag for each environmental measurement is also reported, representing if any gap-filled measurements were used in the computation of a soil flux. Within the soil flux-gradient method, several different approaches can be used to derive a surface flux (Maier & Schack-Kirchner, 2014); the `neonSoilFlux` package reports four different possible values for soil surface flux (Section 4.2.3).

4.2.1 Gap-filling routine

NEON reports QA flags as binary values for each measurement and half-hourly interval. For a given half-hour, if any input variable (soil CO_2 concentration, soil temperature, or soil moisture) at depth z is flagged, computation of F_S is not possible. To address this, flagged measurements and their uncertainties were replaced with a bootstrapped monthly mean ($\overline{m}$) and monthly standard deviation ($\overline{s}$) (Efron & Tibshirani, 1994).

For each month, depth z, and variable, we computed bootstrapped estimates of $\overline{m}$ and $\overline{s}$ from the vectors of unflagged measurements ($\mathbf{m}$), reported standard errors (σ), and the 95%

confidence interval (ϵ, or expanded uncertainty; Farrance & Frenkel (2012)). We also defined a bias vector $\mathbf{b} = \sqrt{\epsilon^2 - \sigma^2}$, which quantifies the spread of uncertainty in a given period and is incorporated into $\overline{m}$. Each of these vectors $(\mathbf{m}, \sigma, \epsilon, \mathbf{b})$.

From these, 5000 bootstrap samples were generated for $\mathbf{m}, \sigma$, and $\mathbf{b}$. For each sample (m_k, b_k, σ_k), we generated a vector $\mathbf{n}$ (length $N = 5000$) by drawing from a normal distribution with mean $m_k + b_k$ and standard deviation σ_k. The sample mean and standard deviation were then computed from $\mathbf{n}$. The resulting distributions of sample means and sample standard deviations provided the bootstrapped monthly mean ($\overline{m}$) and standard error ($\overline{s}$) respectively.

This gap-filling procedure provides a consistent treatment across all data streams. However, alternative approaches may be better suited for longer gaps (e.g., correlations with other NEON measurement levels or soil plots) or for variable-specific conditions. We discuss the effect of gap-filling on our results in Section 6.1.

4.2.2 Soil diffusivity

Soil diffusivity D_a at a given measurement depth is the product of the diffusivity in free air $D_{a,0}$ (m^2 s^{-1}) and the tortuosity ξ (no units) (Millington & Shearer, 1971).

We compute $D_{a,0}$ with Equation 1:

$$D_{a,0} = 0.0000147 \cdot \left(\frac{T_i + 273.15}{293.15} \right)^{1.75} \cdot \left(\frac{P}{101.3} \right) \tag{1}$$

where T_i is soil temperature (°C) at depth i (National Ecological Observatory Network (NEON), 2024d) and P surface barometric pressure (kPa) (National Ecological Observatory Network (NEON), 2024a).

Previous studies by Sallam et al. (1984) and Tang et al. (2003) demonstrated the sensitivity of modeled F_S depending on the tortuosity model (ξ) used to compute diffusivity. At low soil water content, the choice of tortuosity model can lead to order-of-magnitude differences in D_a, which in turn affect modeled F_S. The `neonSoilFlux` package currently includes two approaches to calculate ξ, representing the range of tortuosity behavior reported in Sallam et al. (1984).

The first approach is the Millington-Quirk model (Millington & Shearer, 1971), in which tortuosity depends on both porosity and soil water content:

$$\xi = \frac{(\phi - SWC_i)^{10/3}}{\phi^2} \tag{2}$$

In Equation 2, SWC is the soil water content at depth i (National Ecological Observatory Network (NEON), 2024e) and ϕ is the porosity, which in turn is a function of soil physical properties (National Ecological Observatory Network (NEON), 2024c):

$$\phi = \left(1 - \frac{\rho_s}{\rho_m}\right)(1 - f_V) \tag{3}$$

In Equation 3, ρ_m is the particle density of mineral soil (2.65 g cm^{-3}), ρ_s the soil bulk density (g cm^{-3}) excluding coarse fragments greater than 2 mm (National Ecological Observatory Network (NEON), 2024c), and f_V is a site-specific value that accounts for the proportion of soil fragments between 2-20 mm. Soil fragments greater than 20 mm were not estimated due to limitations in the amount of soil that can be analyzed (National Ecological Observatory Network (NEON), 2024c). We assume that rock fragments contain no internal pores.

The Millington-Quirk model assumes ξ is modulated by the amount of fluid saturation in soil pores (Millington & Shearer, 1971). In contrast, the Marshall model (Marshall, 1959) expresses tortuosity as only a function of porosity ($\xi = \phi^{1.5}$), with ϕ defined from Equation 3. The Marshall model is independent of soil water content and assumes tortuosity is only governed by soil structure. The `neonSoilFlux` package allows users to choose the tortuosity model most appropriate for site-specific conditions and research goals.

4.2.3 Soil flux computation

We applied Fick's law (Equation 4) to compute the soil flux F_{ij} (μmol m^{-2} s^{-1}) across two soil depths i and j:

$$F_{ij} = -D_a \frac{dC}{dz} \tag{4}$$

where D_a is the diffusivity (m^2 s^{-1}) and $\frac{dC}{dz}$ is the gradient of CO_2 molar concentration (μmol m^{-3}, so the gradient has units of μmol m^{-3} m^{-1}). The soil surface flux is theoretically defined by applying Equation 4 to measurements collected at the soil surface and directly below the surface. Measurements of soil temperature, soil water content, and soil CO_2 molar concentration across the soil profile allow for application of Equation 4 across different soil depths. Each site had three measurement layers, so we denote the flux between which two layers as a three-digit subscript F_{ijk} with indicator variables i, j, and k indicate if a given layer was used (written in order of increasing depth), according to the following:

- F_{000} is a surface flux estimate using the intercept of the linear regression of D_a with depth and the slope from the linear regression of CO_2 with depth (which represents $\dfrac{dC}{dz}$ in Fick's Law). Tang et al. (2003) used this approach to compute fluxes in an oak-grass savannah.

- F_{110}, F_{011} are fluxes across the two most shallow layers and two deepest layers respectively. The diffusivity used in Fick's Law is always at the deeper measurement layer. When used as a surface flux estimate we assume CO_2 remains constant above this flux depth.
- F_{101} is a surface flux estimate using linear extrapolation using concentration measurements between the shallowest and deepest measurement layer. Hirano et al. (2003) and Tang et al. (2005) used an approach similar to F_{101} in a temperate deciduous broadleaf forest and ponderosa pine forest respectively.

Uncertainty in all F_{ijk} is computed through quadrature (Taylor, 2022).

4.3 Post processing evaluation

Following collection of field measurements and calculation of the soil fluxes from `neonSoilFlux` package, we compared measured F_S based on closed-dynamic chamber measurements with the LI-COR instruments to a given soil flux calculation from `neonSoilFlux` for each site and flux computation method. Statistics included the associated R^2 value, root mean squared error (RMSE), slope from a linear regression (m), normalized root mean square error.

Finally, for a half-hourly interval we also computed a *post hoc* D_a using the LI-COR flux along with the CO_2 surface gradient reported by NEON using the measurement levels closest to the surface.

Table 2: Summary of measured soil characteristics and flux results from field measurements across six NEON sites using a LI-COR 6800 (LI-870/8250 measurements omitted to enable direct comparability) via the closed-dynamic chamber method. Numeric values for soil CO_2 flux, soil temperature, and volumetric soil water content (VSWC) are the mean and standard deviation of field measurements at each site.

Site	Flux μmol m^{-2} s^{-1}	Soil temp °C	VSWC cm^3 cm^{-3}	n
UNDE	2.55 ± 0.26	14.33 ± 0.77	0.33 ± 0.02	61
WOOD	3.02 ± 0.4	16.01 ± 1.54	0.28 ± 0.01	53
WREF	3.62 ± 0.3	15.34 ± 1.76	0.27 ± 0.06	21
KONZ	6.35 ± 0.97	27.28 ± 4.14	0.37 ± 0.01	44
SJER	0.94 ± 0.02	41.68 ± 11.22	0.01 ± 0.01	32
SRER	0.72 ± 0.09	47.64 ± 7.46	0.04 ± 0.01	32

5 Results

5.1 Concordance between modelled and measured soil CO_2 flux

The sites we visited ranged substantially in both their annual average temperature and precipitation as well as their biome type (Table 2). These differences also influenced the wide range of observed flux rates across sites.

The timeseries of the measured fluxes from the LI-COR 6800 and 870/8250 were compared to modeled soil fluxes from the `neonSoilFlux` R package (Figure 4). We also assessed year-long estimated flux time series and compared those to field measurements made at each site (Figure 5). Results are reported in local time. Where applicable, sites are displayed from left to right by increasing soil temperature (Table 1). Positive values of the flux indicate that there is a flux moving towards the surface. Overall, with the exception of SRER (discussed later) the computed fluxes determined using a variety of plausible methods spanned the field-measured fluxes, but the specific flux-gradient method that best approximated field measurements varied by site.

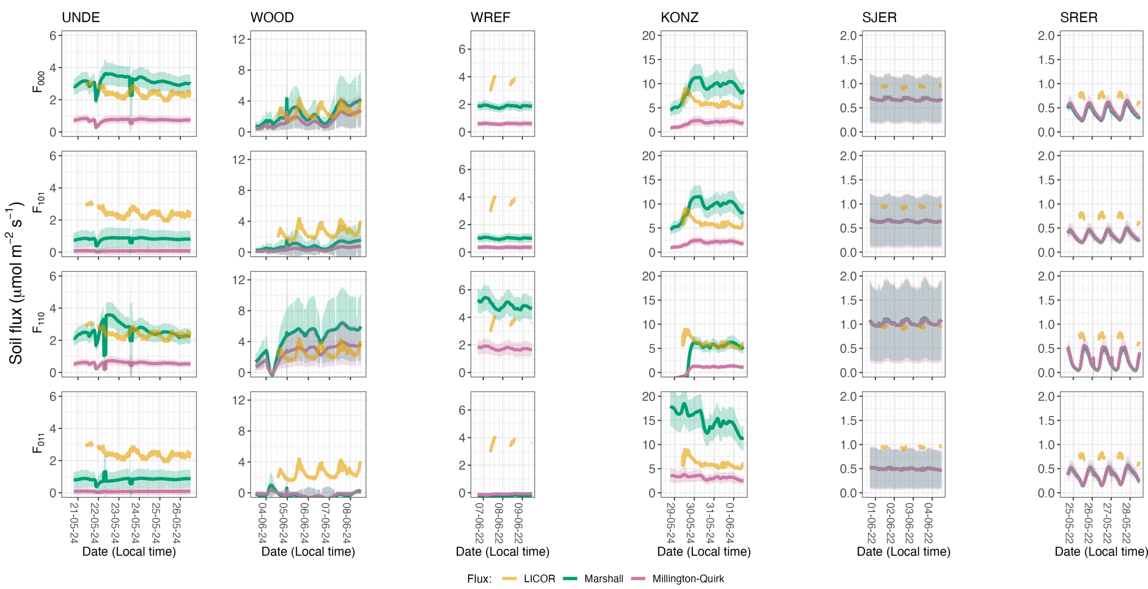

Figure 4: Timeseries of soil surface flux (F_S) from LICOR measured (yellow lines) and modeled soil fluxes (green or purple lines) by the **neonSoilFlux** R package. Fluxes from the **neonSoilFlux** R package are separated by the diffusivity model used (Millington-Quirk or Marshall, Section 4.2.2). Individual vertical axis labels in the first column represent the measurement levels where the flux-gradient approach is applied (Section 4.2.3). Ribbons for modeled soil fluxes represent $\pm$ 1 standard deviation. Results are reported in local time.

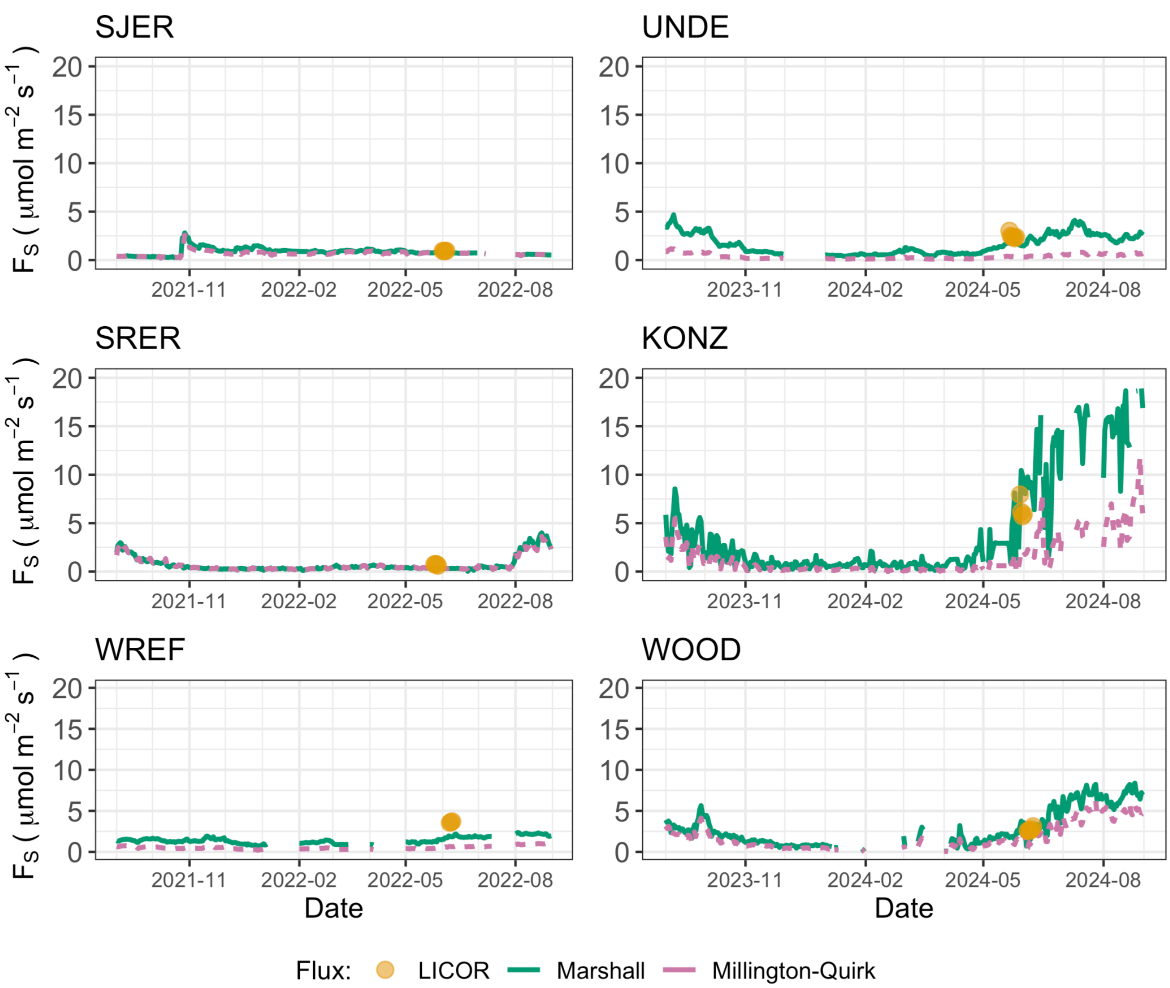

Figure 5: Timeseries of both daily-averaged field F_S (yellow circles) and daily ensemble averaged soil fluxes (average of F_{000}, F_{101}, F_{011}, F_{110}, Section 4.2.3) by the `neonSoilFlux` R package, separated by the diffusivity model used (green or purple lines, Millington-Quirk or Marshall, Section 4.2.2).

We computed the soil fluxes measured by `neonSoilFlux` with the LICOR measured fluxes at that within that half-hourly period, and then calculated the statistical 1-1 comparison between the two. Statistics for each are reported in Table 3.

5.2 Effects of method choice on diffusivity estimates

In four of six field sites, the *post hoc* D_a estimate fell roughly between the two diffusion estimation methods; however this was less the case in the two driest sites, SJER and SRER (Table 1), where the field estimate of diffusivity was either lower or higher than both of the other methods (Figure 6).

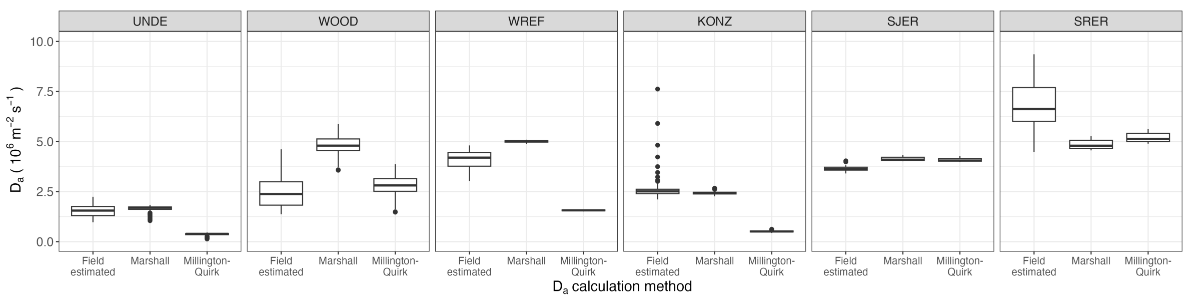

Figure 6: Distribution of diffusivity (D_a) at each study site. Values of D_a were provided by the `neonSoilFlux` package, computed from the Millington-Quirk or Marshall models (Section 4.2.2). A post-hoc estimate of diffusivity (labeled as "Field estimated") was computed through the field measured flux (Figure 4), divided by the CO_2 gradient from the measurement levels closest to the soil surface, as reported by NEON. We only used F_S measured by the LICOR 6800 at all sites to standardize comparisons.

6 Discussion

This study presents a unified data science workflow to efficiently process automated measurements of belowground soil CO_2 concentrations, soil water content, and soil temperature to infer estimates of soil surface CO_2 effluxes through application of Fick's Law (Equation 4).

Table 3: Statistical comparison between measured fluxes at each site with fluxes reported by `neonSoilFlux` with the different diffusivity calculations applied. m refers to the slope of a linear regression between the LICOR measured fluxes at each site and the outputs from `neonSoilFlux`. * = significance at the 5% level, ** = significance at the 1% level. NRMSE is the normalized root mean square error between measured and `neonSoilFlux` outputs, normalized by the sample mean of the LICOR measured fluxes.

	Millington-Quirk			Marshall		
	m	NRMSE	R^2	m	NRMSE	R^2
KONZ						
F_{110}	-0.39**	0.87	0.41	-1.86**	0.63	0.41
F_{101}	-0.12**	0.69	0.22	-0.44**	0.60	0.15
F_{011}	0.16**	0.52	0.20	1**	1.35	0.25
F_{000}	-0.12**	0.70	0.23	-0.41**	0.58	0.14
SJER						
F_{110}	-0.7*	0.13	0.17	-0.76*	0.14	0.18
F_{101}	-0.23*	0.32	0.21	-0.25**	0.31	0.24
F_{011}	-0.07	0.49	0.02	-0.09	0.48	0.03
F_{000}	-0.33*	0.29	0.17	-0.37*	0.28	0.18
SRER						
F_{110}	-0.06	0.56	0.00	-0.05	0.59	0.00
F_{101}	-0.34**	0.66	0.53	-0.33**	0.67	0.52
F_{011}	-0.44**	0.69	0.49	-0.42**	0.70	0.49
F_{000}	-0.48**	0.58	0.51	-0.44**	0.61	0.51
UNDE						
F_{110}	-0.09**	0.77	0.06	-0.29*	0.25	0.02
F_{101}	-0.01**	0.97	0.10	-0.1**	0.66	0.14
F_{011}	-0.01**	0.97	0.05	-0.09**	0.66	0.04
F_{000}	-0.11**	0.70	0.16	-0.29**	0.36	0.06
WOOD						
F_{110}	0.27**	0.31	0.10	0.32**	0.97	0.06
F_{101}	0.11**	0.87	0.16	0.19**	0.69	0.13
F_{011}	0.1**	1.12	0.10	0.23**	1.24	0.11
F_{000}	0.39**	0.47	0.16	0.55**	0.36	0.15
WREF						
F_{110}	-0.17**	0.53	0.78	-0.52**	0.35	0.75
F_{101}	-0.02*	0.91	0.24	-0.05**	0.73	0.35
F_{011}	0.05**	1.03	0.37	0.16**	1.07	0.37
F_{000}	0	0.84	0.00	-0.03	0.49	0.05

Our core goals in this study were: (1) to generate estimates of soil flux from continuous soil sensor data at terrestrial NEON sites using the flux-gradient method and then (2) to compare those estimates to field-measured fluxes based on the closed chamber approach at six NEON focal sites. We discuss our progress toward these core goals through (1) an overall evaluation of the flux-gradient approach (and uncertainty calculation) and (2) site-specific evaluation of differences in estimated vs measured fluxes.

6.1 General evaluation of flux-gradient approach

Key assumptions of the flux-gradient approach are that CO_2 concentrations increase throughout the soil profile such that the highest concentrations are observed in the deepest layers. Additionally, field flux measurements should correlate with F_{000} because they represent surface fluxes. Periods where this gradient condition are not met generally are connected to processes that occur during soil wetting events, where more shallow soil layers produce higher concentrations of CO_2 due to microbial respiration pulses following rewetting. This effect is likely to be largest at sites with rich organic soils (e.g. KONZ). Based on this reasoning, in these types of situations we would *a priori* expect F_{011} (deepest layers) $\leq F_{101} \leq F_{110}$ (shallow layers) $\leq$ F_{000} (all layers) because the previous flux estimates rely primarily on CO_2 concentrations at deeper depths, and could miss high concentrations of CO_2 produced in shallower layers.

When modeling soil respiration, typically a non-linear response function that also considers soil type is used (Bouma & Bryla, 2000; Yan et al., 2016, 2018). For the `neonSoilFlux` package, soil type is connected to the measurement of bulk density, which was characterized at each NEON site. This bulk density estimate is based on replicate samples collected from the site megapit at a subset of soil horizons, with an estimated uncertainty of $\pm 5\%$ (National Ecological Observatory Network (NEON), 2024c). Coarse fragment estimates also have very large uncertainties, but because the volume fraction tends to be low in surface soils it probably wouldn't contribute much additional flux uncertainty.

Our results suggest that the most important way to improve reliability of the flux estimate is to reduce the usage of gap-filled data. The current approach to gap filling in `neonSoilFlux` uses monthly mean data to gap fill—this approach decreases the ability of the estimate to be responsive to short turn pulses that occur with rapid weather shifts. Four sites (KONZ, SRER, WREF, and UNDE) had more than 75% of half-hourly periods with no-gap filled measurements (Figure S1, Supplementary Information). Two sites (SJER and WOOD) had more than 75% of half-hourly intervals with just one gap-filled measurement. While we did not need to use gap-filled measurements to compute the flux at WREF, field data collection occurred following a severe rainstorm, with soils at the beginning of the sampling week near their water holding capacity. We recommend that whenever possible, knowledge of local field conditions should influence analysis decisions in addition to any QA filtering protocols in the `neonSoilFlux` package.

We recognize that this gap-filling approach may lead to gap-filled values that are quite different from the actual values, such as an underestimate of soil moisture following rain events. Further extensions of the gap filling method could use more sophisticated gap-filling routines, similar to what is used for net ecosystem carbon exchange (Falge et al., 2001; Liu et al., 2023; Mariethoz et al., 2015; Moffat et al., 2007; Zhang et al., 2023). The current gap-filling routine provides a consistent approach that can be applied to each data stream, but further work may explore alternative gap-filling approaches.

6.2 Evaluation of flux-gradient approach at each site

Derived results from the `neonSoilFlux` package have patterns that are broadly consistent with those directly measured in the field (Figure 4 and Figure 5), even though statistical comparisons between the field-measured and `neonSoilFlux` values were quite variable and poor (e.g. R^2 ranging from 0.00 to 0.78; Table 3). One advantage of the `neonSoilFlux` package is its ability to calculate fluxes across different soil depths (Figure 3), which allows for additional site-specific customization. We believe the package can provide a useful baseline estimate of soil fluxes that can always be complemented through additional field measurements.

The six locations studied provide a range of case studies that suggest different considerations may apply to different sites when applying the flux-gradient method. For example, the Santa Rita Experimental Range (SRER) is a desert site characterized by sandy soil, which also was the location of the highest field soil temperatures that we observed (Table 2). At SRER the flux across the top two layers (F_{110}) produced a pattern of soil flux most consistent with the observed field data. The remaining methods F_{101}, F_{011}, or F_{000} are derived from information taken from the deepest layer, which seems to have been decoupled from the surface layers both in terms of temperature and CO_2 concentration. This may be a general circumstance where there are large diurnal temperature extremes that rapidly change during the course of a day and overnight, leading to lags in the timing of when temperature increases propagate down to deeper soil layers.

Immediately prior to our visit to Konza Prarie (KONZ), that site that experienced a significant rain event that led to wet soils that gradually dried out over the course of our time there. This pulse of precipitation increased the soil CO_2 concentration at the top layer above the concentrations in lower layers, leading to negative estimated flux values at the start of the experiment. In this case it was only when the soil began to return to a baseline level that the assumptions of the flux-gradient method were again met.

Both of the previous cases also provide context for the poor statistical comparisons between field-measured soil fluxes and `neonSoilFlux` outputs Table 3. When considering systematic deployment of this method across a measurement network, there are a number of independent challenges that require careful consideration. There are clear tradeoffs between (1) accuracy of modeled fluxes (defined here as closeness to field-measured F_S and the uncertainty reduction factor ϵ), (2) precision (which could be defined by the signal to noise ratio), and (3) the choice of the diffusivity model (Section 4.2.2) or flux computation method (Section 4.2.3). A sensitivity analysis (Figure S2, Supplemental Information) found that flux output uncertainty was dominated by measurement uncertainty (T_S, P, SWC, or CO_2) rather than the diffusivity method to compute soil flux. Notably, the F_{110} method was least sensitivty to measurement uncertainty likely because it best aligns with surface chamber measurement assumptions.

Finally, comparing the effects of different diffusivity estimation methods on the match between modeled and measured fluxes (Figure 5) highlights the sensitivity of F_{ijk} to diffusivity. The comparison between diffusivity estimates compared to field estimated diffusivity (Figure 6) demonstrates that site parameters can dictate which measure of diffusivity is most likely to be accurate in a given environmental context. Site-specific differences a largely a reflection of differences in soil moisture across the sites (Table 1), as not all diffusivity estimation methods incorporate soil moisture equivalently. While we here have compares two approaches to calculate diffusivity (the Millington-Quirk and Marshall models), it may be valuable to evaluate other diffusivity models (e.g. the Moldrup model; Moldrup et al. (1999)) as well. Ultimately the choice of a particular diffusivity model could be determined based on knowledge of site-specific evaluations or a set of these models could be used to generate a model ensemble average as a means to trade precision for a more general approach.

6.3 Recommendations for future method development

The `neonSoilFlux` package provides several approaches to estimate soil flux using the gradient method. We believe these approaches enable the software to be used across a range of site-specific assumptions (Maier & Schack-Kirchner, 2014). We note, however, that this choice can have a determinative approach on the calculated values. Ensemble averaging approaches (Elshall et al., 2018; Raftery et al., 2005) may be one way to address this problem if the goal is to calculate fluxes using the same method at a diverse range of different sites. Two other ideas would be to apply machine learning algorithms (e.g. random forests) to generate a single flux estimate across diverse sites, or using co-located estimates of net ecosystem carbon exchange from eddy-flux towers to further constrain results or to assess soil flux results for plausibility (Phillips et al., 2017).

These challenges notwithstanding, the method used here and made available in the `neonSoilFlux` R package has the potential to produce nearly continuous estimates of flux across all terrestrial NEON sites. These estimates are a significant improvement on available approaches to constrain the portion of ecosystem respiration attributable to the soil. This, in turn, also aids in our ability to understand the soil contribution to the net ecosystem flux measured at these sites using the co-located eddy flux towers.

7 Conclusions

We used the R package `neonSoilFlux` to test its broader application in estimating soil CO_2 fluxes with the flux-gradient method, using data from continuous buried soil sensors at NEON terrestrial sites. We compared the predicted fluxes to those measured directly using a field-based closed chamber approach. Soil fluxes from `neonSoilFlux` were broadly effective at producing estimates of flux comparable to those measured in the field using a chamber-based technique. However `neonSoilFlux` outputs are quite sensitive to a number of issues, including: missing data (and thus gap-filling of input measurement datasets), the selection of soil depths used to best calculate the gradient (which may vary between sites), and finally the choice of method used for estimating soil diffusivity. The flexibility of the `neonSoilFlux` package allows the user to evaluate each of these issues with site-specific knowledge and contexts. Future refinements and subsequent validation of `neonSoilFlux` outputs will feed forward into evaluating soil carbon fluxes broader spatial scales to enhance understanding of the ways in which soils across diverse ecosystems are responding to a changing climate.

Sources Cited

Baldocchi, D. (2014). Measuring fluxes of trace gases and energy between ecosystems and the atmosphere - the state and future of the eddy covariance method. *Global Change Biology*, *20*(12), 3600–3609. https://doi.org/10.1111/gcb.12649

Berenbaum, M. R., Carpenter, S. R., Hampton, S. E., Running, S. W., & Stanzione, D. C. (2015). *Report from the NSF BIO Advisory Committee Subcommittee on NEON Scope Impacts*.

Bond-Lamberty, B. (2018). New Techniques and Data for Understanding the Global Soil Respiration Flux. *Earth's Future*, *6*(9), 1176–1180. https://doi.org/10.1029/2018EF000866

Bond-Lamberty, B., Ballantyne, A., Berryman, E., Fluet-Chouinard, E., Jian, J., Morris, K. A., Rey, A., & Vargas, R. (2024). Twenty Years of Progress, Challenges, and Opportunities in Measuring and Understanding Soil Respiration. *Journal of Geophysical Research: Biogeosciences*, *129*(2), e2023JG007637. https://doi.org/10.1029/2023JG007637

Bond-Lamberty, B., Christianson, D. S., Malhotra, A., Pennington, S. C., Sihi, D., AghaKouchak, A., Anjileli, H., Altaf Arain, M., Armesto, J. J., Ashraf, S., Ataka, M., Baldocchi, D., Andrew Black, T., Buchmann, N., Carbone, M. S., Chang, S.-C., Crill, P., Curtis, P.

S., Davidson, E. A., … Zou, J. (2020). COSORE: A community database for continuous soil respiration and other soil-atmosphere greenhouse gas flux data. *Global Change Biology*, *26*(12), 7268–7283. https://doi.org/10.1111/gcb.15353

Bond-Lamberty, B., & Thomson, A. (2010). A global database of soil respiration data. *Biogeosciences*, *7*(6), 1915–1926. https://doi.org/10.5194/bg-7-1915-2010

Bond-Lamberty, B., Wang, C., & Gower, S. T. (2004). A global relationship between the heterotrophic and autotrophic components of soil respiration? *Global Change Biology*, *10*(10), 1756–1766. https://doi.org/10.1111/j.1365-2486.2004.00816.x

Bouma, T. J., & Bryla, D. R. (2000). On the assessment of root and soil respiration for soils of different textures: Interactions with soil moisture contents and soil CO2 concentrations. *Plant and Soil*, *227*(1), 215–221. https://doi.org/10.1023/A:1026502414977

Chen, H., & Tian, H.-Q. (2005). Does a General Temperature-Dependent Q10 Model of Soil Respiration Exist at Biome and Global Scale? *Journal of Integrative Plant Biology*, *47*(11), 1288–1302. https://doi.org/10.1111/j.1744-7909.2005.00211.x

Davidson, E. A., Janssens, I. A., & Luo, Y. (2006). On the variability of respiration in terrestrial ecosystems: Moving beyond Q10. *Global Change Biology*, *12*, 154–164. https://doi.org/10.1111/j.1365-2486.2005.01065.x

Desai, A. R., Murphy, B. A., Wiesner, S., Thom, J., Butterworth, B. J., Koupaei-Abyazani, N., Muttaqin, A., Paleri, S., Talib, A., Turner, J., Mineau, J., Merrelli, A., Stoy, P., & Davis, K. (2022). Drivers of Decadal Carbon Fluxes Across Temperate Ecosystems. *Journal of Geophysical Research: Biogeosciences*, *127*(12), e2022JG007014. https://doi.org/10.1029/2022JG007014

Efron, B., & Tibshirani, R. J. (1994). *An Introduction to the Bootstrap*. Chapman and Hall/CRC. https://doi.org/10.1201/9780429246593

Elshall, A. S., Ye, M., Pei, Y., Zhang, F., Niu, G.-Y., & Barron-Gafford, G. A. (2018). Relative model score: A scoring rule for evaluating ensemble simulations with application to microbial soil respiration modeling. *Stochastic Environmental Research and Risk Assessment*, *32*(10), 2809–2819. https://doi.org/10.1007/s00477-018-1592-3

Falge, E., Baldocchi, D., Olson, R., Anthoni, P., Aubinet, M., Bernhofer, C., Burba, G., Ceulemans, R., Clement, R., Dolman, H., Granier, A., Gross, P., Grünwald, T., Hollinger, D., Jensen, N.-O., Katul, G., Keronen, P., Kowalski, A., Lai, C. T., … Wofsy, S. (2001). Gap filling strategies for defensible annual sums of net ecosystem exchange. *Agricultural and Forest Meteorology*, *107*(1), 43–69. https://doi.org/10.1016/S0168-1923(00)00225-2

Farrance, I., & Frenkel, R. (2012). Uncertainty of Measurement: A Review of the Rules for Calculating Uncertainty Components through Functional Relationships. *The Clinical Biochemist Reviews*, *33*(2), 49–75.

Friedlingstein, P., O'Sullivan, M., Jones, M. W., Andrew, R. M., Hauck, J., Landschützer, P., Le Quéré, C., Li, H., Luijkx, I. T., Olsen, A., Peters, G. P., Peters, W., Pongratz, J., Schwingshackl, C., Sitch, S., Canadell, J. G., Ciais, P., Jackson, R. B., Alin, S. R., … Zeng, J. (2025). Global Carbon Budget 2024. *Earth System Science Data*, *17*(3), 965–1039. https://doi.org/10.5194/essd-17-965-2025

Hamdi, S., Moyano, F., Sall, S., Bernoux, M., & Chevallier, T. (2013). Synthesis analysis of the temperature sensitivity of soil respiration from laboratory studies in relation to incubation methods and soil conditions. *Soil Biology and Biochemistry*, *58*, 115–126. https://doi.org/10.1016/j.soilbio.2012.11.012

Hirano, T., Kim, H., & Tanaka, Y. (2003). Long-term half-hourly measurement of soil CO2 concentration and soil respiration in a temperate deciduous forest. *Journal of Geophysical Research: Atmospheres*, *108*(D20). https://doi.org/10.1029/2003JD003766

Jackson, R. B., Lajtha, K., Crow, S. E., Hugelius, G., Kramer, M. G., & Piñeiro, G. (2017). The Ecology of Soil Carbon: Pools, Vulnerabilities, and Biotic and Abiotic Controls. *Annual Review of Ecology, Evolution and Systematics*, *48*(Volume 48, 2017), 419–445. https://doi.org/10.1146/annurev-ecolsys-112414-054234

Jian, J., Bailey, V., Dorheim, K., Konings, A. G., Hao, D., Shiklomanov, A. N., Snyder, A., Steele, M., Teramoto, M., Vargas, R., & Bond-Lamberty, B. (2022). Historically inconsistent productivity and respiration fluxes in the global terrestrial carbon cycle. *Nature Communications*, *13*(1), 1733. https://doi.org/10.1038/s41467-022-29391-5

Jian, J., Vargas, R., Anderson-Teixeira, K., Stell, E., Herrmann, V., Horn, M., Kholod, N., Manzon, J., Marchesi, R., Paredes, D., & Bond-Lamberty, B. (2021). A restructured and updated global soil respiration database (SRDB-V5). *Earth System Science Data*, *13*(2), 255–267. https://doi.org/10.5194/essd-13-255-2021

Jiang, J., Feng, L., Hu, J., Liu, H., Zhu, C., Chen, B., & Chen, T. (2024). Global soil respiration predictions with associated uncertainties from different spatio-temporal data subsets. *Ecological Informatics*, *82*, 102777. https://doi.org/10.1016/j.ecoinf.2024.102777

Jobbágy, E. G., & Jackson, R. B. (2000). The Vertical Distribution of Soil Organic Carbon and its Relation to Climate and Vegetation. *Ecological Applications*, *10*(2), 423–436. https://doi.org/10.1890/1051-0761(2000)010%5B0423:TVDOSO%5D2.0.CO;2

Liu, K., Li, X., Wang, S., & Zhang, H. (2023). A robust gap-filling approach for European Space Agency Climate Change Initiative (ESA CCI) soil moisture integrating satellite observations, model-driven knowledge, and spatiotemporal machine learning. *Hydrology and Earth System Sciences*, *27*(2), 577–598. https://doi.org/10.5194/hess-27-577-2023

Lunch, C., Laney, C., Mietkiewicz, N., Sokol, E., Cawley, K., & Network), N. (National. E. O. (2025). *neonUtilities: Utilities for Working with NEON Data*.

Luo, Y., Ogle, K., Tucker, C., Fei, S., Gao, C., LaDeau, S., Clark, J. S., & Schimel, D. S. (2011). Ecological forecasting and data assimilation in a data-rich era. *Ecological Applications*, *21*(5), 1429–1442. https://doi.org/10.1890/09-1275.1

Maier, M., & Schack-Kirchner, H. (2014). Using the gradient method to determine soil gas flux: A review. *Agricultural and Forest Meteorology*, *192–193*, 78–95. https://doi.org/10.1016/j.agrformet.2014.03.006

Mariethoz, G., Linde, N., Jougnot, D., & Rezaee, H. (2015). Feature-preserving interpolation and filtering of environmental time series. *Environmental Modelling & Software*, *72*, 71–76. https://doi.org/10.1016/j.envsoft.2015.07.001

Marshall, T. J. (1959). The Diffusion of Gases Through Porous Media. *Journal of Soil Science*, *10*(1), 79–82. https://doi.org/10.1111/j.1365-2389.1959.tb00667.x

Millington, R. J., & Shearer, R. C. (1971). Diffusion in aggregated porous media. *Soil Science*, *111*(6), 372–378.

Moffat, A. M., Papale, D., Reichstein, M., Hollinger, D. Y., Richardson, A. D., Barr, A. G., Beckstein, C., Braswell, B. H., Churkina, G., Desai, A. R., Falge, E., Gove, J. H., Heimann, M., Hui, D., Jarvis, A. J., Kattge, J., Noormets, A., & Stauch, V. J. (2007). Comprehensive comparison of gap-filling techniques for eddy covariance net carbon fluxes. *Agricultural and Forest Meteorology*, *147*(3), 209–232. https://doi.org/10.1016/j.agrformet.2007.08.011

Moldrup, P., Olesen, T., Yamaguchi, T., Schjønning, P., & Rolston, D. E. (1999). Modeling diffusion and reaction in soils: 9. The Buckingham-Burdine-Campbell equation for gas diffusivity in undisturbed soil. *Soil Science*, *164*(2), 75.

National Ecological Observatory Network (NEON). (2024a). *Barometric pressure (DP1.00004.001)*. National Ecological Observatory Network (NEON). https://doi.org/10.48443/RT4V-KZ04

National Ecological Observatory Network (NEON). (2024b). *Soil CO2 concentration (DP1.00095.001)*. National Ecological Observatory Network (NEON). https://doi.org/10.48443/E7GR-6G94

National Ecological Observatory Network (NEON). (2024c). *Soil physical and chemical properties, Megapit (DP1.00096.001)*. National Ecological Observatory Network (NEON). https://doi.org/10.48443/S6ND-Q840

National Ecological Observatory Network (NEON). (2024d). *Soil temperature (DP1.00041.001)*. National Ecological Observatory Network (NEON). https://doi.org/10.48443/Q24X-PW21

National Ecological Observatory Network (NEON). (2024e). *Soil water content and water salinity (DP1.00094.001)*. National Ecological Observatory Network (NEON). https://doi.org/10.48443/A8VY-Y813

Norman, J. M., Kucharik, C. J., Gower, S. T., Baldocchi, D. D., Crill, P. M., Rayment, M., Savage, K., & Striegl, R. G. (1997). A comparison of six methods for measuring soil-surface carbon dioxide fluxes. *Journal of Geophysical Research: Atmospheres*, *102*(D24), 28771–28777. https://doi.org/10.1029/97JD01440

Phillips, C. L., Bond-Lamberty, B., Desai, A. R., Lavoie, M., Risk, D., Tang, J., Todd-Brown, K., & Vargas, R. (2017). The value of soil respiration measurements for interpreting and modeling terrestrial carbon cycling. *Plant and Soil*, *413*(1), 1–25. https://doi.org/10.1007/s11104-016-3084-x

Raftery, A. E., Gneiting, T., Balabdaoui, F., & Polakowski, M. (2005). *Using Bayesian Model Averaging to Calibrate Forecast Ensembles*. https://doi.org/10.1175/MWR2906.1

Sallam, A., Jury, W. A., & Letey, J. (1984). Measurement of Gas Diffusion Coefficient under Relatively Low Air-filled Porosity. *Soil Science Society of America Journal*, *48*(1), 3–6. https://doi.org/10.2136/sssaj1984.03615995004800010001x

Shao, J., Zhou, X., Luo, Y., Li, B., Aurela, M., Billesbach, D., Blanken, P. D., Bracho, R., Chen, J., Fischer, M., Fu, Y., Gu, L., Han, S., He, Y., Kolb, T., Li, Y., Nagy, Z., Niu, S., Oechel, W. C., … Zhang, J. (2015). Biotic and climatic controls on interannual variability in carbon fluxes across terrestrial ecosystems. *Agricultural and Forest Meteorology*, *205*, 11–22. https://doi.org/10.1016/j.agrformet.2015.02.007

Shao, P., Zeng, X., Moore, D. J. P., & Zeng, X. (2013). Soil microbial respiration from observations and Earth System Models. *Environmental Research Letters*, *8*(3), 034034. https://doi.org/10.1088/1748-9326/8/3/034034

Sihi, D., Gerber, S., Inglett, P. W., & Inglett, K. S. (2016). Comparing models of microbial–substrate interactions and their response to warming. *Biogeosciences*, *13*(6), 1733–1752.

https://doi.org/10.5194/bg-13-1733-2016

Tang, J., Baldocchi, D. D., Qi, Y., & Xu, L. (2003). Assessing soil CO2 efflux using continuous measurements of CO2 profiles in soils with small solid-state sensors. *Agricultural and Forest Meteorology*, *118*(3), 207–220. https://doi.org/10.1016/S0168-1923(03)00112-6

Tang, J., Misson, L., Gershenson, A., Cheng, W., & Goldstein, A. H. (2005). Continuous measurements of soil respiration with and without roots in a ponderosa pine plantation in the Sierra Nevada Mountains. *Agricultural and Forest Meteorology*, *132*(3), 212–227. https://doi.org/10.1016/j.agrformet.2005.07.011

Taylor, J. R. (2022). *An Introduction to Error Analysis: The Study of Uncertainties in Physical Measurements, Third Edition* (3rd ed.). University Science Press.

Yan, Z., Bond-Lamberty, B., Todd-Brown, K. E., Bailey, V. L., Li, S., Liu, C., & Liu, C. (2018). A moisture function of soil heterotrophic respiration that incorporates microscale processes. *Nature Communications*, *9*(1), 2562. https://doi.org/10.1038/s41467-018-04971-6

Yan, Z., Liu, C., Todd-Brown, K. E., Liu, Y., Bond-Lamberty, B., & Bailey, V. L. (2016). Pore-scale investigation on the response of heterotrophic respiration to moisture conditions in heterogeneous soils. *Biogeochemistry*, *131*(1), 121–134. https://doi.org/10.1007/s10533-016-0270-0

Zhang, R., Kim, S., Kim, H., Fang, B., Sharma, A., & Lakshmi, V. (2023). Temporal Gap-Filling of 12-Hourly SMAP Soil Moisture Over the CONUS Using Water Balance Budgeting. *Water Resources Research*, *59*(12), e2023WR034457. https://doi.org/10.1029/2023WR034457

Zobitz, J., Ayres, E., O'Rourke, K., Werbin, Z., Lee, L., Abdi, R., Mehmeti, D., & Xiong, L. (2024). *neonSoilFlux: Compute Soil Carbon Fluxes for the National Ecological Observatory Network Sites*.